

Vacancy clustering and acceptor activation in nitrogen-implanted ZnO

Thomas Moe Børseth,¹ Filip Tuomisto,² Jens S. Christensen,¹ Edouard V. Monakhov,¹
Bengt G. Svensson,¹ and Andrej Yu. Kuznetsov^{1,*}

¹*Department of Physics/Centre for Materials Science and Nanotechnology, University of Oslo,
P.O. Box 1126 Blindern, N-0318 Oslo, Norway*

²*Laboratory of Physics, Helsinki University of Technology, P.O. Box 1100, 02015 TKK, Espoo, Finland*

(Received 2 April 2007; published 11 January 2008)

The role of vacancy clustering and acceptor activation on resistivity evolution in N ion-implanted *n*-type hydrothermally grown bulk ZnO has been investigated by positron annihilation spectroscopy, resistivity measurements, and chemical profiling. Room temperature 220 keV N implantation using doses in the low 10^{15} cm⁻² range induces small and big vacancy clusters containing at least 2 and 3–4 Zn vacancies, respectively. The small clusters are present already in as-implanted samples and remain stable up to 1000 °C with no significant effect on the resistivity evolution. In contrast, formation of the big clusters at 600 °C is associated with a significant increase in the free electron concentration attributed to gettering of amphoteric Li impurities by these clusters. Further annealing at 800 °C results in a dramatic decrease in the free electron concentration correlated with activation of 10^{16} – 10^{17} cm⁻³ acceptors likely to be N and/or Li related. The samples remain *n* type, however, and further annealing at 1000 °C results in passivation of the acceptor states while the big clusters dissociate.

DOI: 10.1103/PhysRevB.77.045204

PACS number(s): 61.72.uj, 61.72.Cc, 61.72.J-, 78.70.Bj

I. INTRODUCTION

The superior properties of ZnO such as a high excitonic binding energy¹ compared to other wide band gap semiconductor materials, e.g., GaN, combined with recent substantial improvements both in epitaxial growth and in the fabrication of single crystal substrates^{2–4} explain the increased attention ZnO has received during the past few years. In particular, ZnO is exploited in various optoelectronic devices, such as laser diodes and light-emitting diodes (LEDs) in the blue-UV range. As-grown ZnO normally exhibits *n*-type conductivity, and our understanding of the acceptor nature in ZnO is limited, in spite of several encouraging reports on successful fabrication of devices requiring *p*-type layers, such as LEDs,^{5–7} field-effect transistors,⁸ and photodiodes.^{8,9} For several reasons, nitrogen has been considered one of the best candidates for *p*-type doping of ZnO and has, therefore, been used in the majority of reports on *p*-type conversion.^{5,6,10–14} Among the group-V acceptor candidates (e.g., N, As, P, Sb), N has, according to theory, the shallowest acceptor level,¹⁵ and its ionic radius is similar to that of oxygen, which it substitutes to act as an acceptor—N_O. Experimental studies have detected nitrogen-related acceptor levels in the range of 120–270 meV above the valence band edge [165 ± 40 meV,¹⁶ 163–196 meV,¹⁷ and 266 meV (Ref. 18)]. Many papers also report on difficulties in achieving *p*-type ZnO using nitrogen.^{10,16,18,19} In particular, the mechanisms for potential compensation and passivation are not fully understood. It has been suggested that N might be passivated either by H (Refs. 20 and 21) or compensated by donorlike molecular nitrogen (N₂).^{21,22} Another cause for compensation may be lithium, which can exhibit both donor- and acceptorlike character in ZnO; occupying zinc sites (Li_{Zn}) it behaves as an acceptor, while on interstitial sites (Li_i) it becomes a donor.^{15,23–28} Thus, showing amphoteric behavior and being present in high concentration in hydrothermally

grown ZnO,^{3,29} Li may be expected to play a significant role for electrical compensation.²⁸ If nitrogen is introduced by ion implantation, in addition to the passivation and compensation mechanisms discussed above, the role of radiation-induced defects and defect clusters must be understood.

In the present paper, we show that defects induced during nitrogen implantation interact with the implanted N and background impurities (specifically Li) resulting in a complex evolution of the electrical properties upon annealing. Based on characterization of structural defects and N/Li chemical profiles, we present a scenario that accounts for this complex resistivity evolution. First, the implantation causes a substantial electrical compensation through the implanted region containing a uniform distribution of small vacancy clusters involving at least two Zn vacancies. Subsequent annealing for 1 h at 600 °C leads to the formation of bigger vacancy clusters involving at least 3–4 Zn vacancies and, simultaneously, a low-resistive *n*-type layer is formed in the implanted region. The reduction in resistivity is attributed primarily to deactivation of Li by the vacancy clusters, while N remains inactive. Further annealing at 800 °C results in a dramatic decrease in the electron concentration correlated with activation of 10^{16} – 10^{17} cm⁻³ acceptors likely to be N and/or Li related. The material remains *n* type, however, and further annealing at 1000 °C results in passivation of the acceptor states while the big clusters dissociate. Interestingly, the small clusters are likely to be present after all the annealing stages and are thus anticipated to have only a minor (if any) effect on the electrical properties. Both the small and big clusters observed are likely to contain oxygen vacancies that are not detectable, unfortunately, by the methods applied in this study.

II. EXPERIMENT

Hydrothermally grown single crystal (0001) ZnO wafers with a size of 1×1 cm² and 0.5 mm thickness have been

used. The wafers were nominally undoped but displayed n -type conductivity with two different resistivities, 1 and $10^3 \Omega \text{ cm}$, labeled as samples A and B. Li was found to be a contaminant in both wafers with a concentration of $\sim 5 \times 10^{17} \text{ cm}^{-3}$, unintentionally introduced during the hydrothermal synthesis. The synthesis conditions for A and B were, in principle, similar but they originate from different batches; the difference in electron concentration may be attributed to (i) variations in relative concentrations of intrinsic donor-type defects, e.g., interstitial Zn (Zn_i), (ii) variations in H concentration, and (iii) variations in Li lattice locations, i.e., different relative concentrations of Li_{Zn} and Li_i . Both A and B were implanted with $^{14}\text{N}^+$ ions at an energy of $\sim 220 \text{ keV}$ with doses of 1.2×10^{15} and $2.4 \times 10^{15} \text{ N}^+/\text{cm}^2$, respectively, giving a projected range $R_p \sim 330 \text{ nm}$. All the implantations were performed at room temperature. A factor of 2 difference in the nitrogen implantation dose compared to 3 orders of magnitude difference in the initial resistivity in samples A and B is not likely to affect considerably the evolution of electrical properties of the samples but is helpful for a quantitative interpretation of defect reactions taking place in the samples. Both A and B were cut into four pieces, of which one was kept as a reference, and the remaining ones were isochronally (1 h) annealed at 600, 800, and 1000 °C in air using a conventional furnace.

Concentration vs depth profiles of N and of Li were measured by secondary ion mass spectrometry (SIMS) using a Cameca IMS 7f microanalyzer. The primary and secondary ions used were Cs^+ and $(^{14}\text{N} \ ^{16}\text{O})^-$, and O_2^+ and $^7\text{Li}^+$, respectively. To convert the SIMS intensity to concentration values, as-implanted samples were used as references. Depth conversion was made by measuring the crater depth using a surface profilometer and assuming a constant erosion rate.

The electrical properties of the samples before and after annealing were investigated by conventional four-point probe sheet resistance measurements and cross-sectional atomic force microscopy employing scanning spreading resistance microscopy (SSRM) and scanning capacitance microscopy (SCM) modes, using a VEECO D3100 Nanoscope. The cross sections were prepared by manual cleaving, and the SSRM resistance was extracted from the measured current by applying a dc bias between a Ti-Pt covered silicon tip and the sample mounted to the sample holder using conductive silver paste. Only a qualitative interpretation of the SSRM signal variations in terms of carrier concentration change is typically possible because of nonlinearity originating from (i) SSRM signal to resistivity conversion³⁰ and (ii) that resistivity itself is a product of carrier concentration and mobility. In addition, the SSRM signal depends on the contact resistance in the tip-sample circuit and is not identical in different (even sequential) measurements because of, e.g., tip degradation. Thus, we have normalized the different SSRM profiles with respect to the bulk resistivity values measured on the samples' backsides with the four-point probe after each annealing step. Note that the SSRM depth scale cannot be directly compared with, e.g., the SIMS depth scale, as the exact position of the sample edge in the SSRM cross sectional measurements is not well defined. SCM was carried out using a similar circuit as for SSRM but in a differential capacitance-voltage (dC/dV) mode. The sign of the dC/dV

phase depends on the type of the dominating carriers,³¹ which was used to monitor any n - to p -type conversion.

Positron annihilation spectroscopy (PAS) was employed to study open volume defects in the samples, specifically the behavior of zinc vacancy (V_{Zn}) related defects, the dominant radiation-induced defect detected by PAS in ZnO at room temperature.³² Donor-type oxygen vacancies (V_{O}) are also present in the implanted ZnO,³³ but the V_{O} 's positive charge repels positrons so no trapping occurs. PAS is based on positron trapping at neutral and negative vacancy-type defects, which modifies the annihilation characteristics including the Doppler broadening of the 511 keV annihilation line. The Doppler spectra are evaluated by the conventional line shape parameters representing the fractions of annihilations with low momentum valence electrons (S) and high momentum core electrons (W). Typically, open volume defects are seen as an increase (decrease) in the S (W) parameter.³⁴ The measured S and W parameters are superpositions of contributions from different positron annihilation states. In the case when only two positron states are active, the corresponding data points fall on the line connecting the parameters specific to these states in a W - S plot. In this study, most measurements were performed at room temperature using a variable-energy positron beam in the 0–38 keV range. The Doppler broadening of the annihilation radiation was measured using a Ge detector with an energy resolution of 1.24 keV at 511 keV. The S and W parameters were chosen as $|E_{\gamma} - 511 \text{ keV}| < 0.8 \text{ keV}$ and $2.9 \text{ keV} < |E_{\gamma} - 511 \text{ keV}| < 7.4 \text{ keV}$, respectively, and the values presented in this paper are normalized to those of a vapor-phase grown ZnO reference sample having a very low concentration of defects trapping positrons at room temperature ($S_{\text{ref}}=0.418$, $W_{\text{ref}}=0.0740$).³² Some selected samples were subjected to PAS measurements at different temperatures in the 200–500 K range. Such measurements may reveal the presence of negatively charged ions, i.e., acceptors, since that would result in a characteristic change in the S and W parameters as a function of temperature. At low temperatures, positrons can get trapped at acceptors in shallow Rydberg-type states,^{34,35} decreasing the S and increasing the W values closer to the bulk values. When the temperature increases, the positrons are likely to escape from the negative ions because of a low binding energy $\leq 100 \text{ meV}$ and get trapped at vacancy-type defects increasing the S and decreasing the W parameters toward the characteristic vacancy values.

III. RESULTS

A. Nitrogen and lithium depth profiling

Figure 1 shows N and Li depth profiles for samples A (left) and B (right) before and after annealing. It is readily seen that nitrogen is a very slow diffuser in ZnO having a diffusivity $\leq 10^{-15} \text{ cm}^2/\text{s}$ based on an estimated maximum diffusion length of 10 nm (close to the SIMS's depth resolution) after 1 h annealing at 1000 °C. The deep tail in the nitrogen profile is due to ion channeling. Li atoms, on the other hand, remaining at the background concentration after implantation, redistribute significantly in the region around

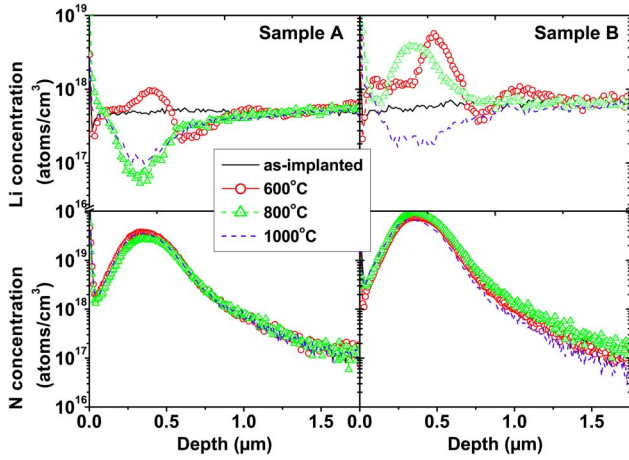


FIG. 1. (Color online) Concentration versus depth profiles of Li (top) and N (bottom) in samples A (left) and B (right) before and after annealing as measured by SIMS.

R_p already after 600 °C annealing where three distinct regions are observed: (i) a near-surface region having uniform Li concentration similar to that in the bulk, (ii) a Li-rich region at the depth around the maximum of the implanted N profile, and (iii) a Li-lean region before reaching the bulk value. The shape of the Li profiles is similar in both samples, although in sample B the regions are more clearly resolved. For sample A, further heat treatment removes Li from region (ii) and a Li-lean region is formed in the major part of the nitrogen-implanted region (excluding the channeling tail). At the minimum, the Li concentration decreases by an order of magnitude to $\sim 5 \times 10^{16} \text{ cm}^{-3}$ at the depth corresponding to the maximum nitrogen concentration after 800 °C annealing. For sample B on the other hand, after 800 °C, the Li profile becomes similar in shape and position to the N profile. After further treatment at 1000 °C, the shape and width of the Li-lean region is preserved in sample A, although the minimum Li concentration increases to $\sim 10^{17} \text{ cm}^{-3}$, whereas in sample B a similar but wider Li-lean region is formed compared to A.

B. Evolution of the electrical properties

Figure 2 shows SSRM resistance profiles from samples A (top) and B (bottom) before and after annealing. As mentioned in Sec. II, the SSRM resistance signals in the unimplanted parts of the profiles are normalized with respect to the backside resistivity values, indicating that some resistivity variation takes place in the bulk ZnO because of the postimplant heat treatment. The variations in the bulk resistivity level may have different origins at different temperatures. For example, the bulk resistivity increase at 600 °C may be because of H outdiffusion,³⁶ whereas further changes at higher temperatures are more likely related to reconstruction of intrinsic defects. Note that the bulk resistivity variations are much less compared with the dramatic resistivity evolution in the implanted regions. For sample A, the SSRM signal in the implanted region first increases by more than 4 orders of magnitude and then after annealing at 600 °C, the

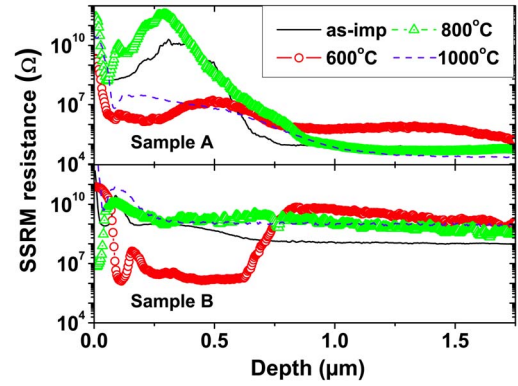


FIG. 2. (Color online) SSRM resistance versus depth profiles of N-implanted ZnO for samples A (top) and B (bottom).

signal drops to a level close to the bulk value. Then, after 800 °C, the resistance increases again by more than 5 orders of magnitude. Finally, after 1000 °C, the signal in the implanted region is reduced to a level of ~ 100 times the bulk value. The initial higher bulk resistivity in sample B provides a different picture for the evolution of the SSRM signals in the implanted region. First, only a slight increase in the SSRM signal is observed and then it decreases by 4 orders of magnitude after 600 °C, before increasing back to the substrate value after 800 °C. The final 1000 °C treatment does not change the signal significantly. For all the treatments, no signs of *p*-type conversion were observed according to the SCM dC/dV phase (not shown).

C. Vacancy related defects

Figure 3 shows depth profiles of the *S*-parameter extracted from typical Doppler broadening spectra for samples A and B before and after annealing. In the as-implanted samples,

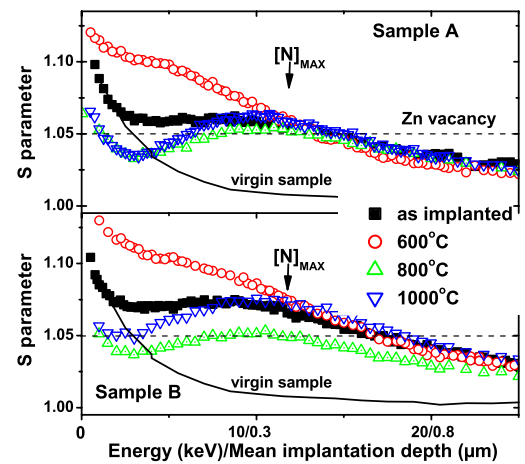


FIG. 3. (Color online) Doppler spectroscopy data for the N-implanted samples: *S* parameter as a function of positron implantation energy for samples A (top) and B (bottom). The dashed line indicates the V_{Zn} -specific *S* parameter, given in Ref. 32. $[N]_{\text{MAX}}$ corresponds to the position of the N peak concentration in accordance with SIMS.

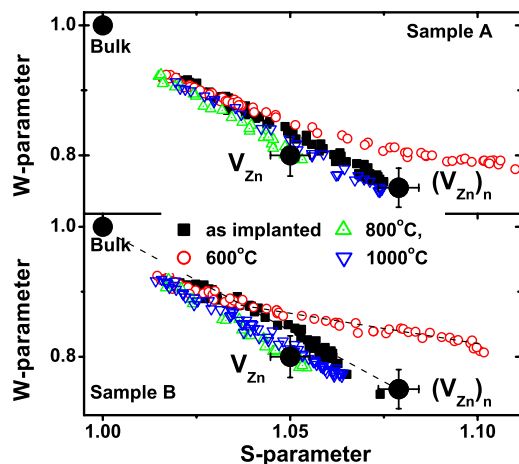


FIG. 4. (Color online) Doppler spectroscopy W - S plots for the N-implanted samples: W parameter as function of S parameter for samples A (top) and B (bottom). The S and W parameters corresponding to positron annihilation at V_{Zn} are from Ref. 32.

vacancy clusters having an open volume larger than that of the Zn monovacancy are clearly indicated in the near-surface region by the S -parameter plateaus above the characteristic V_{Zn} level,³² Fig. 3 and this holds, in particular, for the high dose sample B. In the following, we refer to these small clusters as $(V_{Zn})_n$. The dose dependent increase of the plateau level in the as-implanted sample B compared to that in sample A is an additional argument for V_{Zn} clustering. Indeed, if the observed S -parameter value in sample A simply corresponded to saturation trapping at V_{Zn} , there would be no dose dependence. After annealing at 600 °C, the S -parameter increases substantially in the near-surface region in both samples. The high S -parameter value, well above the level corresponding to saturation trapping by V_{Zn} , indicates the presence of big vacancy clusters $(V_{Zn})_N$ with open volume larger than that for $(V_{Zn})_n$ observed right after implantation, i.e., $N > n$. After 800 °C, the S -parameter decreases substantially, Fig. 3, indicating that (i) both $(V_{Zn})_n$ and $(V_{Zn})_N$ disappear or (ii) positrons predominantly annihilate at other defects, possibly negatively charged impurities and/or defects suppressing trapping at vacancy clusters. Interestingly, after 1000 °C, the S -parameter increases again in the region of maximum N concentration where it reaches a level similar to that in the as-implanted samples, Fig. 3, also showing a clear dose dependence indicating the presence of $(V_{Zn})_n$. Thus, it is likely that $(V_{Zn})_n$ remain after all the annealing steps, but after 800 °C, the S parameter is determined in accordance with hypothesis (ii).

IV. ANALYSIS OF Zn-VACANCY CLUSTERING AND EVIDENCE OF ACCEPTOR ACTIVATION AT 800 °C

As discussed in Sec. III C, vacancy clustering takes place in both samples A and B resulting in two different types of clusters, $(V_{Zn})_n$ and $(V_{Zn})_N$, depending on the annealing conditions. Figure 4 shows W - S plots and indeed, based on the slope of corresponding data points in the W - S plots, we es-

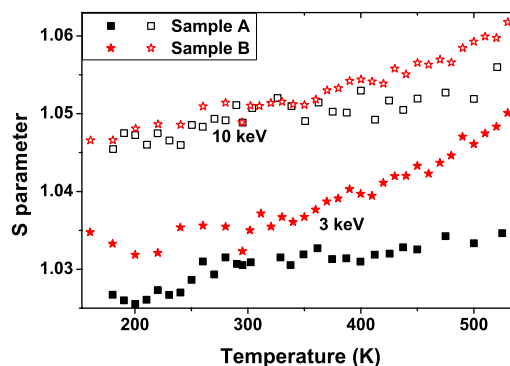


FIG. 5. (Color online) Doppler broadening S parameter as function of measurement temperature for N-implanted samples annealed at 800 °C. Closed symbols represent measurements using 3 keV positron implantation energy, corresponding to a mean implantation depth around 100 nm; open symbols represent 10 keV measurements, corresponding to a mean implantation depth similar to the maximum position of the implanted nitrogen profile.

timate that the small clusters contain at least two Zn vacancies. In the as-implanted samples, using an S -parameter value for $(V_{Zn})_n$ of 1.08,³⁷ a bulk lifetime for positrons of ~ 170 ps,³² and a positron trapping coefficient of $\sim 2 \times 10^{15} \text{ s}^{-1}$,³² the $(V_{Zn})_n$ concentration is estimated to $\sim 1 \times 10^{18}$ and $\sim 2 \times 10^{18} \text{ cm}^{-3}$ in samples A and B, respectively.

Analyzing the big clusters observed after 600 °C in Fig. 3 using the corresponding W - S plots in Fig. 4, one can readily see that the data points neither fall on the line connecting the bulk and V_{Zn} nor on that connecting the bulk and $(V_{Zn})_n$ annihilation states. Based on the slope of these cluster points in the W - S plots, $(V_{Zn})_n$ remain after the 600 °C anneal as seen from a double slope for the corresponding data points in the W - S plots, particularly visible for sample B (Fig. 4 lower panel).

Moreover, $(V_{Zn})_n$ are evidently present after 1000 °C as seen from the corresponding data points in Fig. 4, especially visible for sample B where “as-implanted” and “1000 °C” points display very similar lines between the bulk and $(V_{Zn})_n$ annihilation states. Hence, as suggested in Sec. III C, $(V_{Zn})_n$ are likely then to be present also after 800 °C and the observed low S and high W parameters are attributed to predominant annihilation at alternative states present only after the 800 °C anneal. Both small and big clusters are likely to contain oxygen vacancies, but these cannot be quantified by PAS because of their small effect on the total open volume, whereas interstitial oxygen atoms may form volatile molecules. To obtain a further understanding of the defect reconstruction after 800 °C, temperature dependent PAS measurements were performed.

Figure 5 shows results from Doppler broadening measurements undertaken at different sample temperatures after annealing at 800 °C. Two positron energies, 3 and 10 keV, were used in the measurements, the former corresponding to the near-surface region in Fig. 3 showing a weak S -parameter dose dependence and the latter probing the depth corresponding to the maximum N concentration where no dose dependence is observed. The data exhibit a substantial tem-

perature dependence suggesting negatively charged annihilation sites, such as negative ions—acceptors—so that positrons are efficiently trapped in shallow Rydberg states. Thus, at low temperatures, the observed S and W values are superpositions of annihilations at open volume defects, $(V_{\text{Zn}})_n$, and at the negatively charged ions, e.g., N_O^- or Li_{Zn}^- . When the measurement temperature increases toward 500 K, the positrons gain sufficient thermal energy to escape from the acceptors, diffuse until they are trapped by open volume defects, e.g., $(V_{\text{Zn}})_n$, and annihilate. Thus, the annihilation parameters observed at sufficiently high temperature are no longer the superposition of negative ion and vacancy cluster annihilation but are instead characteristic of the vacancy clusters alone. Therefore, the increase in the S parameter with increasing sample temperature in Fig. 5 is consistent with the presence of negatively charged ions after the 800 °C anneal. The effect is more pronounced in the high dose sample B, which suggests that N exists in its ionized acceptor state, N_O^- . In the region probed by the 10 keV positrons, i.e., the peak of the nitrogen profile, the acceptor concentration is estimated to $\sim 10^{16} \text{ cm}^{-3}$ in sample A and $\sim 10^{17} \text{ cm}^{-3}$ in sample B. Note that the difference in N chemical concentration is only a factor of 2, indicating that also other acceptors, e.g., Li_{Zn} , are involved. In addition, the 3 keV measurements reveal the presence of acceptors also close to the surface, although at a lower concentration, and an association with the implanted distribution of N cannot be excluded.

V. MICROSCOPIC MECHANISM FOR THE RESISTIVITY EVOLUTION

As discussed in Sec. III B, no p -type conversion was observed in the samples irrespective of the original electron concentration although evidence for acceptor activation was obtained after 800 °C, providing a hole concentration of $\sim 10^{16} - 10^{17} \text{ cm}^{-3}$. The acceptor action is likely compensated by donor and/or midgap electronic states. Assuming N_O^- to be a dominating acceptor, several mechanisms for the compensation may be put forward, and below, we discuss a model that accounts for the resistivity evolution in Fig. 2.

Prior ion implantation SSRM resistance values of 10^5 and $10^8 \text{ } \Omega$ were measured in samples A and B reflecting the corresponding difference in the free carrier concentration assuming no major variations in the carrier mobility in the samples. After implantation, the resistance increased in sample A by 5 orders of magnitude to $\sim 10^{10} \text{ } \Omega$ at the implantation peak while the corresponding increase in sample B was only 1 order of magnitude (from 10^8 to $10^9 \text{ } \Omega$) despite its higher initial resistance and factor of 2 higher implantation dose (1×10^{15} vs $2 \times 10^{15} \text{ N/cm}^2$). This result is surprising and suggests that the as-grown sample B contains a high concentration of compensating defects and/or impurities that interact with implantation induced defects preventing formation of deep level centers and/or yielding passivation of the compensating defects and/or impurities.

The first annealing step at 600 °C results in a considerable increase in both n_A and n_B simultaneous with (i) significant Li redistribution in the implanted region and (ii) an

increase in the S parameter at the shallow side of the implanted profile indicating formation of big vacancy clusters, $(V_{\text{Zn}})_N$. The formation of $(V_{\text{Zn}})_N$ is crucial in the resistivity evolution; first, it may partially consume electrically active midgap defects, and second, as recently shown, $(V_{\text{Zn}})_N$ may trap and deactivate Li.²⁸ Indeed, the Li diffusion observed after 600 °C, Fig. 1, is consistent with Li trapping by the $(V_{\text{Zn}})_N$.

Further annealing at 800 °C leads to a decrease in both n_A and n_B . Most likely, the $(V_{\text{Zn}})_N$ clusters dissociate consistent with the binding energy of $\sim 2.6 \text{ eV}$ previously found in Li- and He-implanted samples.²⁸ In Ref. 28, it was also shown that after $(V_{\text{Zn}})_N$ dissociation, the S parameter decreased to the unimplanted bulk level because V_{Zn} annealed out. In contrast, the S parameter in Fig. 3 does not go down to the reference level and contains contributions from at least two annihilation centers, presumably $(V_{\text{Zn}})_n$ and negatively charged ions, most likely N_O^- and/or Li_{Zn}^- . Effectively, the observed S parameter is given by $S = \eta_{\text{bulk}} S_{\text{bulk}} + \eta_{\text{ion}} S_{\text{ion}} + \eta_{(V_{\text{Zn}})_n} S_{(V_{\text{Zn}})_n}$, with $1 = \eta_{\text{bulk}} + \eta_{\text{ion}} + \eta_{(V_{\text{Zn}})_n}$ where η_{bulk} , η_{ion} , and $\eta_{(V_{\text{Zn}})_n}$ are the fractions annihilating at the different states. Using $S_{(V_{\text{Zn}})_n} \approx 1.08$, we estimate that $\sim 1/3$ of the positrons annihilate at negatively charged ions. Thus, the decrease in n_A and n_B after 800 °C may be at least partially associated with the activation of N_O^- and/or Li_{Zn}^- acceptors.

The presence of negatively charged acceptors after 800 °C annealing is confirmed by the measurements of the temperature dependence of the S parameter (Fig. 5). In sample A, Li is depleted from the implanted region at 800 °C leaving N_O^- as the main candidate for the acceptor activity. In sample B, Li is still at high concentration after 800 °C, so both N_O^- and Li_{Zn}^- may contribute to the decrease of n_B , consistent with the ten times higher acceptor concentration in sample B, as estimated by PAS, compared with only a factor of 2 difference in nitrogen dose. Note that $n_\text{B} > n_\text{A}$ after 800 °C, similar to that in as-implanted samples, Fig. 2, supporting the suggestion that the as-grown sample B contains a high concentration of compensating defects and/or impurities. Further annealing at 1000 °C results in a substantial increase in the S parameter, thus indicating that (i) the acceptors activated at 800 °C become inactive and (ii) a significant fraction of the $(V_{\text{Zn}})_n$ clusters remains stable. The fact that $(V_{\text{Zn}})_n$ are observed after all the annealing stages indicates that they are likely to be electrically inactive. In sample A, the deactivation of acceptors is consistent with the increase in n_A , while in sample B, n_B remains low, possibly because of a higher stability of compensating defects. In addition, it is worthwhile to note that in the present study, we have characterized vacancy related defects only and are not discussing the influence of intrinsic interstitial-like defects.

Finally, the mechanism for the resistivity evolution outlined above is consistent with recent studies on nitrogen doping of ZnO performed by other authors. First, Lin *et al.*¹⁴ reported activation of N acceptors at $\sim 850 \text{ } ^\circ\text{C}$, and second, ionized N_O^- acceptors are known to be metastable and tend to convert to molecular nitrogen at sufficiently high temperature.^{38,39} Our observations are also consistent with previous PAS studies⁴⁰ showing a similar evolution of the S parameter versus annealing temperature, although the

authors⁴⁰ did not consider alternative positron annihilation states at ionized acceptors.

VI. CONCLUSIONS

Room temperature 220 keV N ion implantation into ZnO using doses in the low 10^{15} cm⁻² range induces small and big vacancy clusters containing at least 2 and 3–4 Zn vacancies, respectively. The small clusters are present already in the as-implanted samples and remain stable up to 1000 °C without affecting the electrical properties significantly. In contrast, formation of the big clusters at 600 °C is associated with a substantial increase in the free electron concentration attributed to gettering of amphoteric Li impurities by these clusters. Both small and big clusters are likely to contain oxygen vacancies, but their effect on the total open volume

cannot be quantified by PAS. Further annealing at 800 °C results in a dramatic decrease in the electron concentration correlated with activation of 10^{16} – 10^{17} cm⁻³ acceptors likely to be N and/or Li related. The samples remain *n* type, however, and further annealing at 1000 °C results in passivation of the acceptor states and disappearance of the big clusters.

ACKNOWLEDGMENTS

We thank Mikko Rummukainen and Maija Mattinen at Helsinki University of Technology for initial technical support with positron spectroscopy and assistance with temperature dependent PAS measurements, respectively. Financial support by the University of Oslo through the FUNMAT program, and by NordForsk through the NOCDAD collaboration, is gratefully acknowledged.

*andrej.kuznetsov@fys.uio.no

¹D. G. Thomas, *J. Phys. Chem. Solids* **15**, 86 (1960).

²E. V. Kortunova, P. P. Chvanski, and N. G. Nikolaeva, *J. Phys. IV* **126**, 39 (2005).

³K. Maeda, M. Sato, I. Niikura, and T. Fukuda, *Semicond. Sci. Technol.* **20**, S49 (2005).

⁴D. C. Reynolds, C. W. Litton, D. C. Look, J. E. Hoelscher, B. Clafin, T. C. Collins, J. Nause, and B. Nemeth, *J. Appl. Phys.* **95**, 4802 (2004).

⁵A. Tsukazaki *et al.*, *Nat. Mater.* **4**, 42 (2005).

⁶A. Tsukazaki, M. Kubota, A. Ohtomo, T. Onuma, K. Ohtani, H. Ohno, S. F. Chichibu, and M. Kawasaki, *Jpn. J. Appl. Phys., Part 2* **44**, L643 (2005).

⁷W. Liu *et al.*, *Appl. Phys. Lett.* **88**, 092101 (2006).

⁸Y. R. Ryu, T. S. Lee, J. A. Lubguban, H. W. White, Y. S. Park, and C. J. Youn, *Appl. Phys. Lett.* **87**, 153504 (2005).

⁹L. J. Mandalapu, Z. Yang, F. X. Xiu, D. T. Zhao, and J. L. Liu, *Appl. Phys. Lett.* **88**, 092103 (2006).

¹⁰T. M. Barnes, K. Olson, and C. A. Wolden, *Appl. Phys. Lett.* **86**, 112112 (2005).

¹¹J. M. Bian, X. M. Li, C. Y. Zhang, W. D. Yu, and X. D. Gao, *Appl. Phys. Lett.* **85**, 4070 (2004).

¹²A. B. M. Ashrafi, I. Suemune, H. Kumano, and S. Tanaka, *Jpn. J. Appl. Phys., Part 2* **41**, L1281 (2002).

¹³A. N. Georgobiani, A. N. Gruzintsev, V. T. Volkov, M. O. Vorobiev, V. I. Demin, and V. A. Dravin, *Nucl. Instrum. Methods Phys. Res. A* **514**, 117 (2003).

¹⁴C.-C. Lin, S.-Y. Chen, S.-Y. Cheng, and H.-Y. Lee, *Appl. Phys. Lett.* **84**, 5040 (2004).

¹⁵C. H. Park, S. B. Zhang, and S. H. Wei, *Phys. Rev. B* **66**, 073202 (2002).

¹⁶F. Reuss, C. Kirchner, T. Gruber, R. Kling, S. Maschek, W. Limmer, A. Waag, and P. Ziemann, *J. Appl. Phys.* **95**, 3385 (2004).

¹⁷A. Zeuner, H. Alves, D. M. Hofmann, B. K. Meyer, A. Hoffmann, U. Habocek, M. Strassburg, and M. Dworzak, *Phys. Status Solidi B* **234**, R7 (2002).

¹⁸K. Tamura *et al.*, *Solid State Commun.* **127**, 265 (2003).

¹⁹K. Iwata, P. Fons, A. Yamada, K. Matsubara, and S. Niki, *J. Cryst. Growth* **209**, 526 (2000).

²⁰X. Li, B. Keyes, S. Asher, S. B. Zhang, S. H. Wei, T. J. Coutts, S. Limpijumngong, and C. G. Van de Walle, *Appl. Phys. Lett.* **86**, 122107 (2005).

²¹S. Limpijumngong, X. Li, S.-H. Wei, and S. B. Zhang, *Physica B* **376-377**, 686 (2006).

²²E. C. Lee, Y. S. Kim, Y. G. Jin, and K. J. Chang, *Phys. Rev. B* **64**, 085120 (2001).

²³J. J. Lander, *J. Phys. Chem. Solids* **15**, 324 (1960).

²⁴D. Zwingel, *J. Lumin.* **5**, 385 (1972).

²⁵E. C. Lee and K. J. Chang, *Phys. Rev. B* **70**, 115210 (2004).

²⁶M. G. Wardle, J. P. Goss, and P. R. Briddon, *Phys. Rev. B* **71**, 155205 (2005).

²⁷N. Y. Garces, L. Wang, N. C. Giles, L. E. Halliburton, D. C. Look, and D. C. Reynolds, *J. Electron. Mater.* **32**, 766 (2003).

²⁸T. Moe Børseth, F. Tuomisto, J. S. Christensen, W. Skorupa, E. V. Monakhov, B. G. Svensson, and A. Y. Kuznetsov, *Phys. Rev. B* **74**, 161202(R) (2006).

²⁹L. E. Halliburton, L. Wang, L. Bai, N. Y. Garces, N. C. Giles, M. J. Callahan, and B. Wang, *J. Appl. Phys.* **96**, 7168 (2004).

³⁰M. Stangioni, M. Ciappa, and W. Fichtner, *Microelectron. Reliab.* **45**, 1532 (2005).

³¹C. C. Williams, *Annu. Rev. Mater. Sci.* **29**, 471 (1999).

³²F. Tuomisto, V. Ranki, K. Saarinen, and D. C. Look, *Phys. Rev. Lett.* **91**, 205502 (2003).

³³F. Tuomisto, K. Saarinen, D. C. Look, and G. C. Farlow, *Phys. Rev. B* **72**, 085206 (2005).

³⁴K. Saarinen, P. Hautojärvi, and C. Corbel, in *Identification of Defects in Semiconductors*, edited by M. Stavola (Academic, New York, 1998), p. 209.

³⁵K. Saarinen *et al.*, *Phys. Rev. Lett.* **79**, 3030 (1997).

³⁶K. Ip, M. E. Overberg, Y. W. Heo, D. P. Norton, S. J. Pearton, S. O. Kucheyev, C. Jagadish, J. S. Williams, R. G. Wilson, and J. M. Zavada, *Appl. Phys. Lett.* **81**, 3996 (2002).

³⁷Note that the actual values for the saturation trapping at $(V_{Zn})_n$ may be higher than 1.08. Higher dose implantations may resolve this. We use the 1.08 value as the best approximation.

³⁸P. Fons, H. Tampo, A. V. Kolobov, M. Ohkubo, S. Niki, J. Tomimaga, R. Carboni, F. Boscherini, and S. Friedrich, *Phys. Rev. Lett.* **96**, 045504 (2006).

³⁹P. Fons, H. Tampo, S. Niki, A. V. Kolobov, M. Ohkubo, J. Tomimaga, S. Friedrich, R. Carboni, and F. Boscherini, *Nucl. Instrum. Methods Phys. Res. B* **246**, 75 (2006).

⁴⁰Z. Q. Chen, M. Maekawa, A. Kawasuso, R. Suzuki, and T. Ohdaira, *Appl. Phys. Lett.* **87**, 091910 (2005).